Communication

Grain Refinement of a Large-Scale Al Alloy Casting by Introducing the Multiple Ultrasonic Generators During Solidification

RUIQING LI, ZHILIN LIU, FANG DONG, XIAOQIAN LI, and PINGHU CHEN

Based on the multiple ultrasonic generators, a new technique was reported to produce the large-scale Al alloy castings for downstream deformation processing. The effects of different configurations of ultrasonic generators on the degree and homogeneity of grain refinement were investigated during solidification. Experimental results show that a grain-refined structure with reduced macrosegregation was obtained in the large-scale cylindrical Al alloy ingot (650 mm in diameter, 4800 mm in length). Meanwhile, the role of ultrasonic treatment in the production of large-scale castings was discussed. Additionally, these results raise some new questions regarding the relationship between ultrasonic physics and grain refinement, which require further studies.

DOI: 10.1007/s11661-016-3576-6

The large-scale Al alloy ingots, with fine microstructures, are the fundamental raw materials to manufacture the "large-scale complex component" through extensive deformation, which is widely used in aerospace, transportation, and energy-saving applications. Currently, the direct chill semi-continuous (DCS) casting of Al alloy is considered as one major technological method to produce large-scale castings. However, in the DCS casting of high-strength Al alloy, solidification becomes complex owing to the difficulties, *i.e.,* large-scale temperature gradient, thermal stress, and convection. Such difficulties will lead to the inhomogeneous distribution of microstructures and solutes, resulting in severe cracking and macrosegregation. Therefore, the prerequisite to obtain the high-quality "large-scale complex components," which are homogeneous, fine-grained, and non-cracking, is to develop advanced casting technology. Currently, adding grain refiners and/or applying physical stirring are used to improve the casting quality. Extensive work has already been conducted in the grain refinement of Al, Mg, and Zn alloys;[1–3] however, these studies were mainly focused on small-scale ingots. In terms of adding grain refiners, the quantity increases largely with increasing the size of casting, which may increase cost and contamination in casting. The physical methods include mechanical stirring,[4–6] electromagnetic stirring,[7] ultrasonic vibration,[8,9] and gas bubbles.[10] For electromagnetic stirring, the electric energy also increases simultaneously with increasing the size of casting, which can bring potential safety issues. These methods are not suitable for large-scale casting.

Normally, in the large-scale casting, the ultrasonic treatment is applied to manipulate the solidification process.[9] The positive contribution of ultrasonic treatment, in refining Al, Mg, Zn, and Sn and their alloys, has been well verified.[11–18] In recent two decades, many researchers investigated the effect of single ultrasonic treatment on solidification. For instance, Wang *et al.* introduced ultrasonic vibration in Al-Cu alloys. It was found that both grain sizes and solute segregation were reduced/modified.[11] After ultrasonic treatment in A356 Al alloys, Jian *et al.*[12] and Xu *et al.*,[13] respectively, observed that (a) the dendrite grains were transformed into equiaxed grains, and (b) the amount of shrinkage was reduced. Alternatively, Qian *et al.* and Liu *et al.* studied the contribution of ultrasonic treatment on the solidification of Mg alloys.[14–17] Moreover, Eskin systematically investigated the relationship between ultrasonic treatment and Al solidification.[9] It was found that the ultrasonic treatment generated favorable merits, *i.e.,* grain refinement, degassing, increased solute solubility, and reduced segregation. However, most of these studies focused on elucidating the role of single ultrasonic treatment in the small-scale casting, which was applied for civil products. Regarding those large-scale castings (the diameter of ingots exceeds 550 mm), the single ultrasonic treatment cannot induce satisfying results. In this paper, three ultrasonic generators were used to manipulate solidification/microstructures of the cylindrical 2219 Al ingots with a diameter of 650 mm. Through optimizing the configuration parameters of three ultrasonic generators, the influence of ultrasonic configuration (in the 3-D volume of crystallizer) on both the solidification microstructures and the solute macrosegregation was investigated.

The experimental material was 2219 Al alloy, *i.e.,* Al-6.2Cu-0.36Mn-0.11Zr-0.1V-0.10Fe-0.06Si-0.01Mg-0.10Zn-0.05wt pct Ti. Unless specified otherwise, all element contents were expressed in weight percent. The

RUIQING LI, FANG DONG, and PINGHU CHEN, Ph.D. Students, ZHILIN LIU, Lecturer, and XIAOQIAN LI, Professor, are with the College of Mechanical and Electrical Engineering, Central South University, Changsha 410083, P.R. China, and also with the State Key Laboratory of High Performance Complex Manufacturing, Changsha 410083, P.R. China. Contact e-mail: zhilin.liu@csu.edu.cn
Manuscript submitted March 20, 2016.
Article published online May 26, 2016

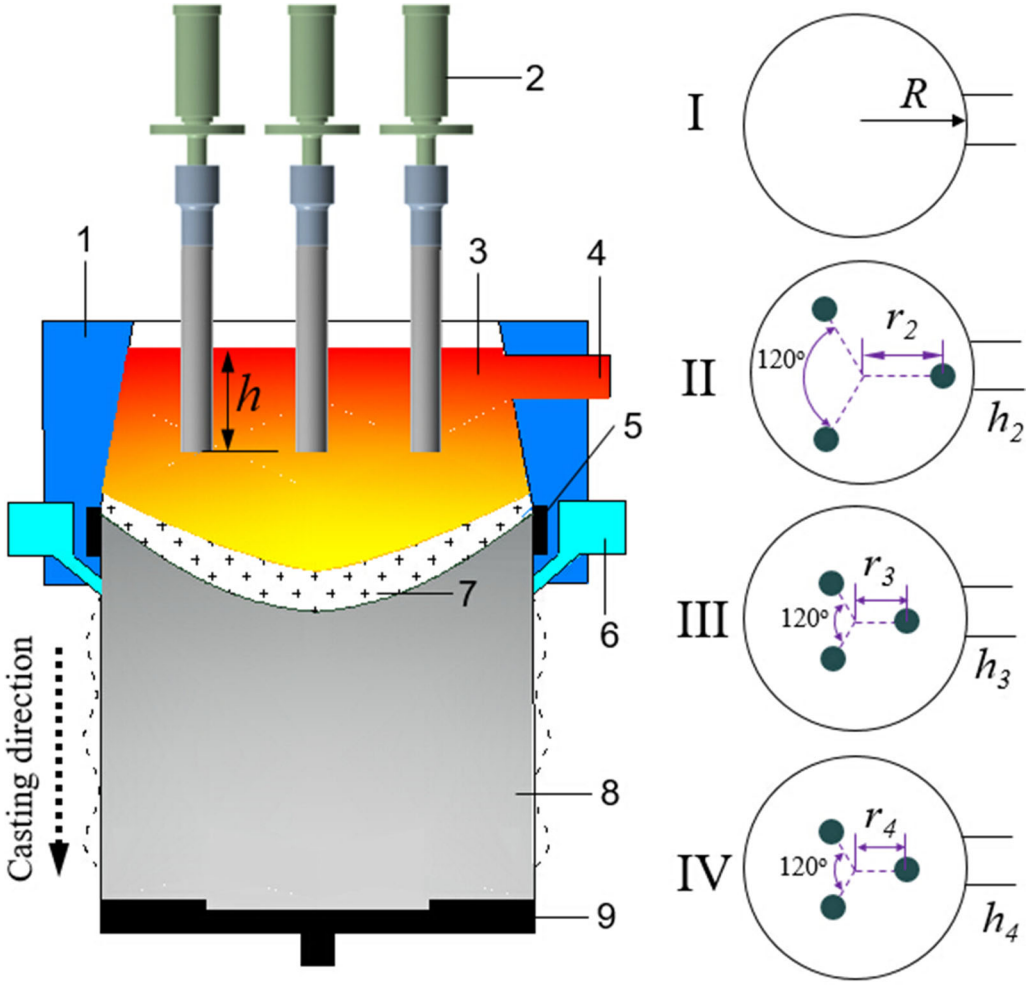

Fig. 1—Schematic configuration of the multiple ultrasonic generators in the direct chill (DC) large-scale castings: 1-mold with a hot top, 2-ultrasonic generator, 3-melt, 4-launder, 5-crystallizer, 6-cooling system, 7-mushy zone, 8-solidified ingot, 9-dummy plate. The three ultrasonic generators were symmetrically placed in three forms of configurations, *i.e.,* II, III, and IV (on the right). As a reference, there was no ultrasonic treatment in I. The values of R, r_2, r_3, r_4, h_2, h_3, and h_4 are 325, 240, 150, 150, 100, 200, and 200 mm, respectively. h represents the depth from the melt surface to liquid.

2219 Al alloys were melted in an electrical resistance furnace, followed by removing the dross, stirring, degassing, and filtering. The whole melting process of 2219 Al alloy was carried out in a protective atmosphere of argon. Combined with spinning nozzle inert gas flotation (SNIF®), a fumeless inline degassing (FILD®) method was applied for melt refining. Then, the alloy melts were introduced into the casting system, as shown in Figure 1. During solidification, the cooling water flowed around the crystallizer and was sprayed on the surface of solid ingot until the casting was completed. The frequency of all three ultrasonic generators is 20 ± 1 kHz, the corresponding power is 1 kW, and the peak-to-peak amplitude is 20 ± 1.0 μm. When the casting length reached 1400, 2400, and 3400 mm, the configuration methods of three ultrasonic generators in Figures 1(II) through (IV) were accordingly used. The final length and the diameter of 2219 Al alloy ingots were 4800 and 650 mm, respectively.

Four groups of metallurgical specimens were transversely cut at different lengths of the large-scale cylindrical ingots, as shown in Figure 2(a). Then, these specimens were well prepared for chemical analysis and microstructural examination. The thickness and diameter of all four cylindrical specimens are 50 and 650 mm, respectively. To reveal the grain morphology, metallographic specimens were etched using the Keller solution (1 pct HF, 1.5 pct HCl, and 2.5 vol pct HNO_3) and examined in a Leica® optical microscope fitted with image analysis software. Average grain sizes (d) on the cross section of each specimen, measured by a linear intercept technique (ASTM 112-10), were used to assess the refining efficiency. Whenever possible, depending on the microstructure, nine fields from each sample were examined and over 80 counts were achieved in each field. Meanwhile, the macrosegregation on each specimen was determined by a spark spectrum analyzer (Spectromax) accordingly, which is the same as that used by Eskin *et al.*[19] In order to obtain detailed macrosegregation information, some random specimens were further examined using scanning electron microscopy (SEM; TESCAN, MIRA 3 LMH/LMU)

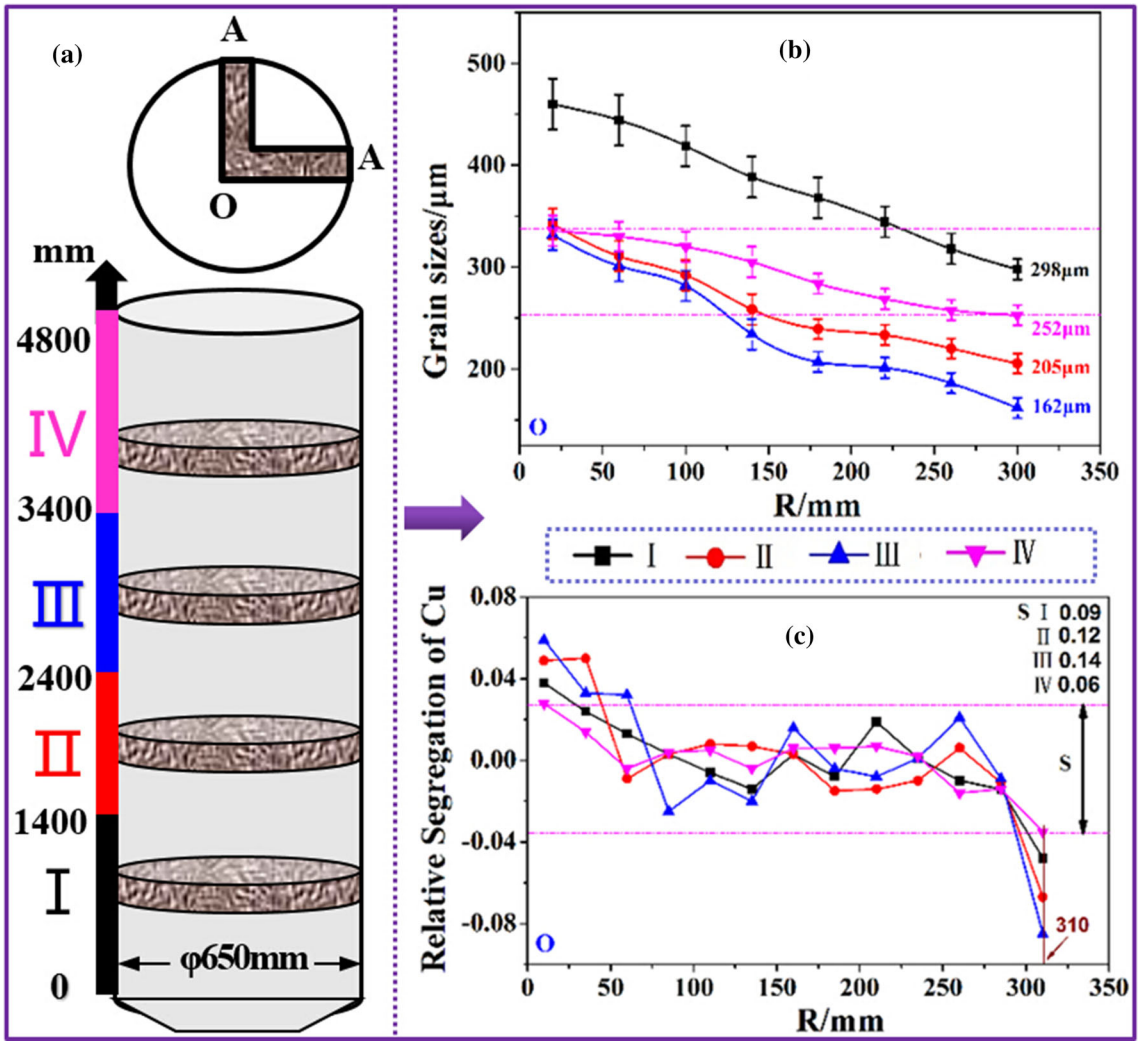

Fig. 2—(*a*) Illustration of the different sampling positions on the large-scale 2219 alloy ingot, (*b*) the measured averaged grain sizes at different sampling positions, and (*c*) the determined macrosegregation of Cu at different sampling positions. The samples extracted from the same positions have the same color. I, II, III, and IV in (a) correspond to the casting methods in Figs. 1(I) through (IV), respectively. In the horizontal axis of (b) and (c), 0 and 350 mm represent the positions from center to edge in each ingot.

equipped with energy-dispersive X-ray spectroscopy (EDS).

The measured results are illustrated in Figures 2(b) and (c). It can be seen in Figure 2(b) that the largest d values occurred in the center of large-scale ingots in the four groups of samples. Then, the d values decreased gradually to the minimum values at the edge of large-scale ingots. After introducing the proposed novel ultrasonic technique, the d values at the center of ingots were reduced from 460 to 340 μm. Meanwhile, the d values at the edge of ingots in groups II, III, and IV were decreased from 298 to 205, 162, and 252 μm, respectively. Figure 2(c) shows the macrosegregation of Cu in the radial direction of cylindrical specimen. Similar trend in all the specimens with and without ultrasonic treatment was observed that (i) the positive macrosegregation primarily formed at the center, (ii) the negative macrosegregation developed at the edge, and (iii) the mixing positive and negative macrosegregation occurred between the center and the edge. Normally, macrosegregation was characterized using an index S, $S = (C_{max} - C_{min})/C_o$, in which C_{max}, C_{min}, and C_o represent the maximum, minimum, and initial solute contents, respectively.[9] Compared with groups I, II, and III, the macrosegregation of Cu in group IV only fluctuated in a narrower zone (S = 0.06). Moreover, Figure 3 indicates the difference of microstructure in the four groups of specimens. After applying ultrasonic treatment, the dominant coarse grains in the central position of ingots were obviously refined.

Regarding the mechanism of ultrasonic-assisted large-scale casting, it is mainly elucidated by the cavitation effect and the acoustic streaming.[20,21] In liquid metal melts, the cavitation effect can only be generated when a cavitation threshold reaches. Normally, the cavitation threshold in the Al alloy melts at 973.15 K (700.00 °C) is about 1.1 MPa.[22] In this paper, a hot-cap DC casting was used. The difference, between the melt surface and the boundary of mushy zone, was determined to be 395

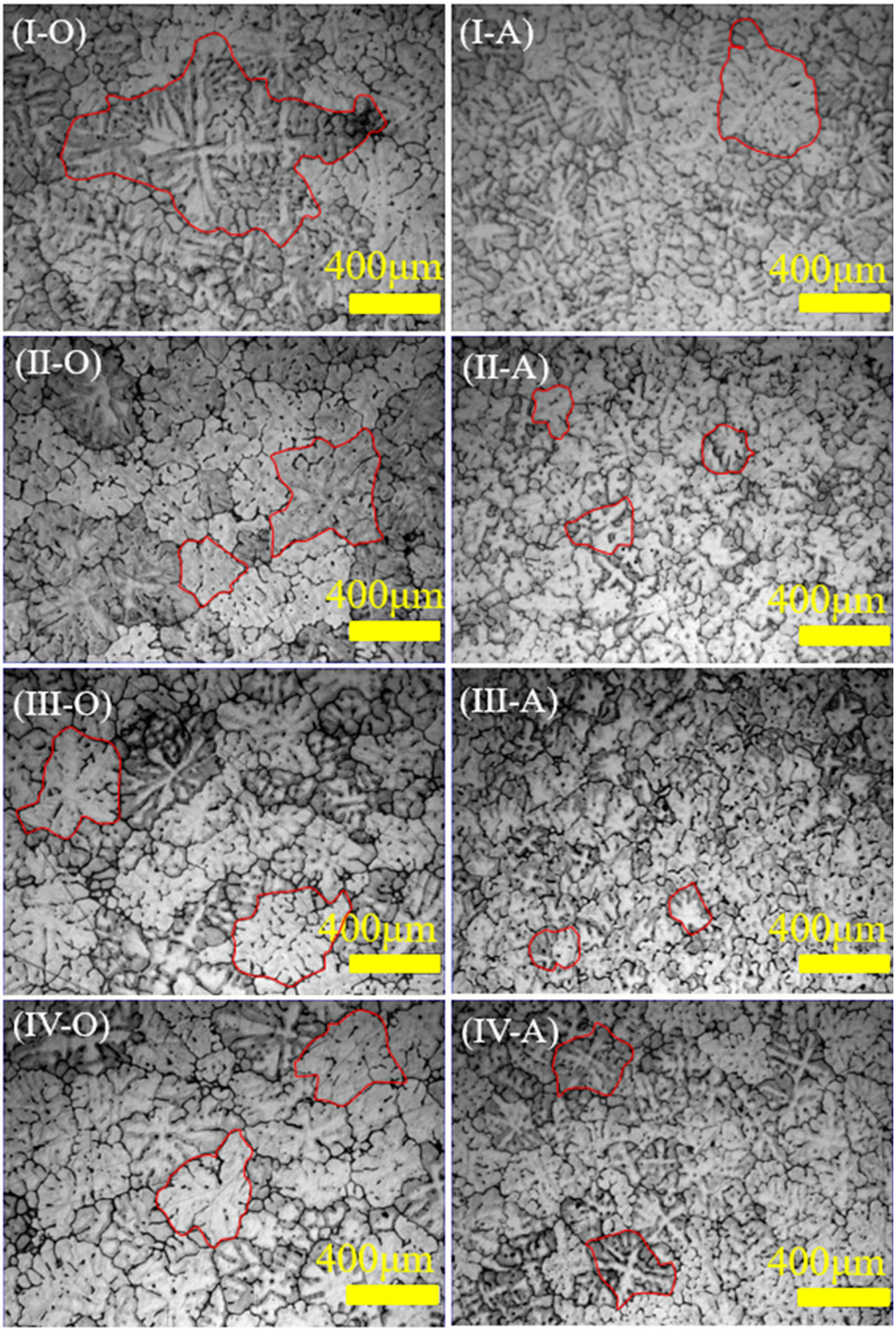

Fig. 3—Microstructures at different positions in the four groups of specimens. I, II, III, and IV represent four groups of specimens. O and A designate the center and the edge positions of each specimen, respectively.

and 230 mm at the center and the edge, respectively. At different depths of the Al melt in the mold, the role of ultrasonic treatment in solidification varied. Thus, the depth of cavitation effect in the Al alloy melt must be calculated. In practice, it is hard to determine the pressure of ultrasonic wave (P_o) in the Al alloy melt at a high temperature. However, P_o can be obtained through measuring its vibration eigenvalue (A_o) in the ambient

Table I. Physical Parameters of Various Mediums That were Used to Transfer the Ultrasonic Wave into the Al Alloy Melts

Parameters	Ultrasonic Rod	Al Alloy Melt	Ambient Air
ρ/(kg m^{-3})	4471.3	2350	1.293
c/(m s^{-1})	4105.1	2282	341

ρ represents the density of various mediums. c is the wave velocity of ultrasonic in corresponding mediums.

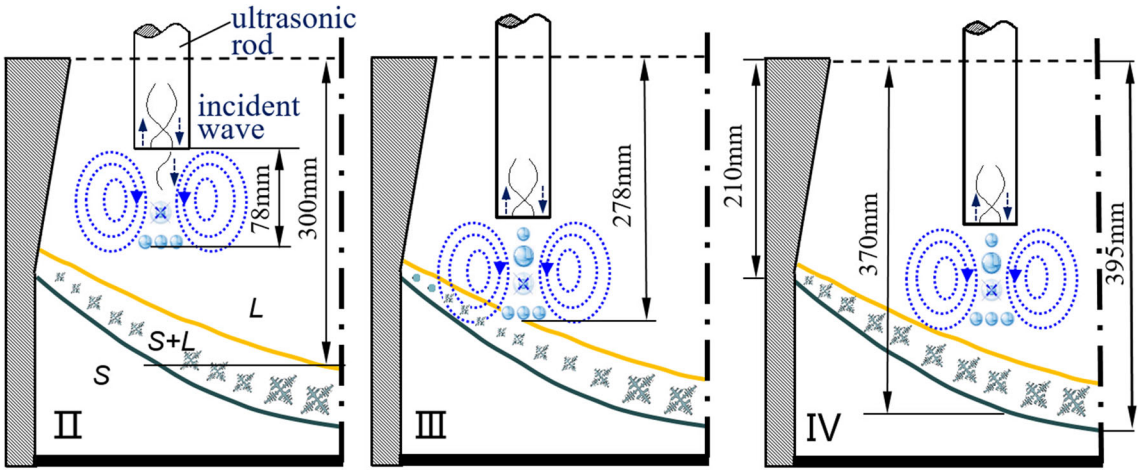

Fig. 4—Multiple ultrasonic-generated cavitation zones in a single period of large-scale casting. II, III, and IV correspond to the three different groups of experimental layout.

environment at room temperature, because the relationship between P_o and A_o can be elucidated by Eq. [1].[6,18]

$$P_o = 2\pi f \cdot \rho_c \cdot A_o, \quad [1]$$

where f and ρ_c designate the frequency and the impedance of ultrasonic wave, respectively. When the ultrasonic wave perpendicularly penetrates the 2219 Al alloy melt, the pressure induced by the transmission ultrasonic wave (P_t) is a function of the incident ultrasonic wave, as expressed in Eq. [2].

$$P_t = P_i \cdot t \quad [2]$$

$$t = 2\rho_t c_t/(\rho_t c_t + \rho_i c_i) \quad [3]$$

In Eqs. [2] and [3], P_i is the pressure induced by the incident ultrasonic wave, t is the transmission coefficient, $\rho_t c_t$ is the impedance of ultrasonic wave in the Al alloy melt, and $\rho_i c_i$ is the impedance of ultrasonic wave in an ultrasonic rod. The physical parameters of the Al alloy melt, the ultrasonic rod, and the ambient air are listed in Table I accordingly. P_t can be calculated through solving Eqs. [1] through [3].

At a given position of the cross section of an ultrasonic rod, the pressure induced by ultrasonic wave (P_z) is quantified using Eq. [4].[23]

$$P_z = 2P_t \sin\left[\frac{\pi}{\lambda}\left(\sqrt{R_s^2 + a^2} - a\right)\right], \quad [4]$$

where a is the distance between a given point and the sound source, λ is the wavelength, P_t is the pressure of transmission ultrasonic wave, and R_s is the radius of cylindrical ultrasonic rod. In this paper, the resonant frequency (f) of an ultrasonic vibration system is equal to 20 kHz, the wavelength (λ) is 0.1141 m, and the radius of cylindrical ultrasonic rod (R_s) is 0.025 m. When P_z reached 1.1 MPa in casting, the depth (a) of cavitation zone was calculated to be 78 mm, as shown in Figure 4(II). In semi-continuous casting, the cavitation zone will evolve periodically. At the steady state in each period, the depth of cavitation zone will be kept at around 78 mm. In this paper, we mainly focused on the steady state in a single period.

The roles of ultrasonic treatment in three different groups of samples are shown in Figure 4. Compared with group IV, the ultrasonic rods in groups II and III were placed more close to the mold inner face, but fixed at different depths in melt. In group II, the ultrasonic rod was fixed at 100 mm below the melt surface, and the cavitation zone boundary is calculated to be around 78 mm (see Figure 4(II)). 78 mm is still above the mushy zone boundary, which implies that the cavitation effect cannot reach the growing microstructures in the mushy zone. Thus, the ultrasonic treatment produced no direct contribution to solidification in the mushy zone in group II. However, due to the continuous ultrasonic energy from ultrasonic generators into melt, the active cavitation bubbles will repeat growing, expanding, compressing, and collapsing, which induces the high-pressure micro-ject flow (MJF). Through ceaselessly impacting the surfaces of potential particles, these MJF can remove/reduce the surface contamination of particles, which improves the wettability of particles as heterogeneous nucleation sites.[24] These nucleation particles may

come from either *in situ* formation or the native potent particles that are present in melts. For instance, it was well documented that the $TiAl_3$, $ZrAl_3$, $NbAl_3$, and/or BTi_2 can serve as efficient nucleation sites.[25–28] The compositions, sizes, crystal structures, and their similarity with the alloy matrix can be found elsewhere.[26–28] Actually, similar phenomena were also reported in Mg-Al alloy[29] and Al-Si alloy.[30] Thus, more potential nucleation particles were activated, resulting in grain refinement. In group III, the ultrasonic rod was fixed at 200 mm below the melt surface, and the cavitation zone boundary intersected the mushy zone boundary (see Figure 4(III)). So the cavitation effect can reach and directly influence the growing microstructures in the mushy zone. Therefore, the contribution of ultrasonic treatment to grain nucleation and growth was obtained in group III.

Moreover, in groups II and III, the ultrasonic rod is close to the mold inner face, so the transmission ultrasonic wave was hindered by both the solid and the mold inner face. Further, the acoustic streaming effect, generated by ultrasonic vibration, was restricted in a relatively small local zone. As a result, the melt flowed inhomogeneously between the center and the edge of large-scale casting, which simultaneously increased the solute gradient of Cu. Then, the larger the solute gradient of Cu evolved, the stronger the macrosegregation of Cu in the large-scale casting became, as shown in Figure 2(c). In group IV, the ultrasonic rods were placed 200 mm below the melt surface as those in group III, but positioned near to the casting center. Meanwhile, the depth of cavitation zone was also calculated to be 278 mm below the melt surface. Although the calculated cavitation zone is similar to that in group III, the acoustic streaming effect was not hindered by the solid and the mold inner face. This is because the ultrasonic rods were positioned near to the casting center. Under this situation in group IV, the ultrasonic-generated acoustic streaming can reach the whole large-scale melt, leading to the enhancement of the homogeneous distribution of solute.[31] Moreover, the active potential nucleation particles can be transferred/moved to more areas in the large-scale casting, which produces grain refinement in both the center and the edge of large-scale ingots. This point was verified by the results in Figures 2(b) through (c) and 3. In group IV, it was well indicated that the microstructures on the whole cross section were grain refined, and the macrosegregation of Cu was smallest among all groups of samples.

In summary, the multiple ultrasonic generators were configured in three different forms, *i.e.,* groups II, III, and IV. Then, their effects on the solidification process in the large-scale 2219 Al casting were investigated accordingly. In the configuration of group IV, the relatively homogeneously distributed microstructures, with pronounced grain refinement and least macrosegregation, were obtained on the whole cross section of large-scale ingots. This was mainly attributed to two reasons. Through reducing the surface contamination of particles, the high-pressure micro-ject flow (generated in group IV) promoted the activation of the heterogeneous nucleation on potent particles, resulting in grain-refined microstructures. Meanwhile, the acoustic streaming effect was not hindered in group IV, so the ultrasonic-generated acoustic streaming reached the whole large-scale melt, leading to the enhancement of the homogeneous distribution of solute. However, the present results also raise some new questions, including (a) what is and how to justify the optimal number of ultrasonic generators that are available in a casting mold, (b) how the metallostatic pressure (metal head) influences cavitation threshold, and (c) what is the relationship between generator's number, casting size, and the average grain sizes. Future work will focus on addressing such questions.

The authors would like to acknowledge the funding support from the National Natural Science Foundation of China (51475480, 51575539) and the National Basic Research Program of China (2012CB619504).

REFERENCES

1. T. Quested and A.L. Greer: *Acta Mater.*, 2005, vol. 53, pp. 4643–53.
2. D.H. StJohn, Q. Ma, M.A. Easton, P. Cao, and Z. Hildebrand: *Metall. Mater. Trans. A*, 2005, vol. 36A, pp. 1669–79.
3. W.K. Krajewski, A.L. Greer, and P.K. Krajewski: *Archives Metall. Mater.*, 2013, vol. 58, pp. 845–47.
4. H.T. Li, Y. Wang, and Z. Fan: *Acta Mater.*, 2012, vol. 60, pp. 1528–37.
5. M.C. Flemings, R.G. Riek, and K.P. Young: *Mater. Sci. Eng.*, 1976, vol. 25, pp. 103–17.
6. Z. Fan, Y. Wang, M. Xia, and S. Arumuganathar: *Acta Mater.*, 2009, vol. 57, pp. 4891–4901.
7. Y.B. Zuo, J.Z. Cui, D. Mou, Q.F. Zhu, X.J. Wang, and L. Li: *Trans. Nonferrous Met. Soc. China*, 2014, vol. 24, pp. 2408–13.
8. F. Wang, D.G. Eskin, T. Connolley, and J.W. Mi: *J. Cryst. Growth*, 2016, vol. 435, pp. 24–30.
9. G.I. Eskin and D.G. Eskin: *Ultrasonic Treatment of Light Alloy Melts*, 2nd ed., CRC Press, Boca Raton, 2014.
10. J. Wannasin, R.A. Martinez, and M.C. Flemings: *Scripta Mater.*, 2006, vol. 55, pp. 115–18.
11. G. Wang, M.S. Darguscha, M. Qian, D.G. Eskin, and D.H. StJohn: *J. Cryst. Growth*, 2014, vol. 408, pp. 119–24.
12. X. Jian, H.B. Xu, T.T. Meek, and Q.Y. Han: *Mater. Lett.*, 2005, vol. 59, pp. 190–93.
13. H.B. Xu, Q.Y. Han, and T.T. Meek: *Mater. Sci. Eng. A*, 2008, vol. 473, pp. 96–104.
14. M. Qian, A. Ramirez, and A. Das: *J. Cryst. Growth*, 2009, vol. 311 (14), pp. 3708–15.
15. M. Qian, A. Ramirez, A. Das, and D.H. StJohn: *J. Cryst. Growth*, 2010, vol. 312 (15), pp. 2267–72.
16. A. Ramirez, M. Qian, B. Davis, T. Wilks, and D.H. StJohn: *Scripta Mater.*, 2008, vol. 59 (1), pp. 19–22.
17. X. Liu, Y. Osawa, S. Takamori, and T. Mukai: *Mater. Lett.*, 2008, vol. 62, pp. 2872–75.
18. Z.L. Liu, D. Qiu, F. Wang, J.A. Taylor, and M.X. Zhang: *Metall. Mater. Trans. A*, 2016, vol. 47A, pp. 830–41.
19. D.G. Eskin, R. Nadella, and L. Katgerman: *Acta Mater.*, 2008, vol. 56 (1), pp. 1358–65.
20. G.I. Eskin: *Zeitschrift fuer Metallkunde*, 2002, vol. 93 (6), pp. 502–07.
21. J.D. Hunt and K.A. Jackson: *J. Appl. Phys.*, 1966, vol. 37 (1), pp. 254–57.

22. K. Yasuda, Y. Saiki, T. Kubo, M. Kuwabara, and J. Yang: *Jpn. J. Appl. Phys*., 2007, vol. 46 (7B), pp. 4939–44.
23. K.M. Li and D.R. Liu: *Ultrasonic-assisted nondestructive testing*, Water Resources and Electric Power Press, Beijing, 1985.
24. G.I. Eskin: *Adv. Perfor. Mater*., 1997, vol. 4 (2), pp. 223–32.
25. M.A. Easton and D.H. StJohn: *Acta Mater*., 2001, vol. 49, pp. 1867–78.
26. F. Wang, Z.L. Liu, D. Qiu, J.A. Taylor, and M.X. Zhang: *Acta Mater*., 2013, vol. 61, pp. 360–70.
27. F. Wang, D. Qiu, Z.L. Liu, J.A. Taylor, and M.X. Zhang: *Acta Mater*., 2013, vol. 61, pp. 5636–45.
28. F. Wang, Z.L. Liu, D. Qiu, J.A. Taylor, and M.X. Zhang: *J. Appl. Cryst*., 2014, vol. 47, pp. 770–79.
29. P. Cao, M. Qian, and D.H. StJohn: *Scripta Mater*., 2005, vol. 53, pp. 841–44.
30. Y. Zhang, H. Zheng, Y. Liu, L. Shi, R. Xu, and X. Tian: *Acta Mater*., 2014, vol. 70, pp. 162–73.
31. D.G. Eskin: *Physical Metallurgy of Direct Chill Casting of Aluminum Alloys*, CRC Press, Boca Raton, 2008.